Journal of Power Sources 189 (2009) 655–659

Contents lists available at ScienceDirect

Journal of Power Sources

journal homepage: www.elsevier.com/locate/jpowsour

Short communication

Electrochemical performance of La–Co–Sn alloys as anode materials for Li-ion batteries

G. Wang[a], Z.W. Lu[a,b], X.P. Gao[a,*], X.J. Liu[b], J.Q. Wang[b]

[a] Institute of New Energy Material Chemistry, Nankai University, Tianjin 300071, China
[b] Tianjin Institute of Power Sources, Tianjin 300381, China

ARTICLE INFO

Article history:
Received 21 June 2008
Received in revised form 2 September 2008
Accepted 15 September 2008
Available online 25 September 2008

Keywords:
La–Co–Sn alloys
Ball milling
Anode material
Li-ion battery

ABSTRACT

Sn-rich La–Co–Sn ternary alloys were obtained by arc-melting process and subsequent ball-milling. X-ray diffraction (XRD) and scanning electron microscopy (SEM) were used to determine the structure and morphology of the obtained alloys. In addition, the galvanoststic discharge/charge test, cyclic voltammetry (CV) and electrochemical impedance spectroscopy (EIS) were carried out to characterize the electrochemical properties of these alloys as anode materials for Li-ion batteries. It is found that all the as-cast La–Co–Sn ternary alloys have the same main phase of $La_3Co_4Sn_{13}$ and low electrochemical capacities. Among these alloys, the as-cast $LaCoSn_4$ alloy exhibits the *best* electrochemical performance. The ball-milling process results in the *reduced* cystallinity, and the enhanced electrochemical capacities as compared to the as-cast alloy. In particular, the $LaCoSn_4$ alloy, obtained after ball-milling for 16 h, provides the higher reversible discharge capacity and the better cycle stability.

1. Introduction

In order to improve the performance of Li-ion batteries, a worldwide effort has been made to find alternative active materials with a high capacity and good cycle stability. Various anode materials with enhanced lithium storage capacities and thermal stabilities were reported for Li-ion batteries in the past decades [1–4]. Among these active materials, tin-based alloys or films have been widely concerned as promising anode materials because of its high theoretical capacity ($Li_{4.4}Sn$, 992 mAh g^{-1}), high tap density and safe thermodynamic potential as compared to the commonly used graphite [5–7]. However, a large volume change of tin-based alloys as active anode materials is accompanied to the lithium alloying/de-alloying process, which could lead to the particle pulverization and rapid capacity decay of the electrode. To improve cycle performance, considerable efforts were made by using tin-based alloys with less active or inactive metal elements such as Ca–Sn [8], Mg–Sn [9], Fe–Sn [10], Ni–Sn [11], Co–Sn [12,13], Cu–Sn [14,15], Sn–Sb [16], Ce–Sn [17], and as well as multi-component Fe–Sn–C composites [18]. The inactive matrix may buffer the large volume expansion of the active tin, as a result, the structure of the electrode can be stabilized during cycling. Recently, tin-based ternary alloys were also developed as anode materials with improved cycle ability [19–24].

Because the limited inner space of lithium ion battery, it is also important to find the composites with the high tap density as anode materials. In our previous work, it is demonstrated that the Si/AB_5 composites with a high tap density, obtained after ball-milling, can deliver a larger reversible capacity and better cycle ability [25]. It is well known that the crystal density of the $La_3Co_4Sn_{13}$ alloy is 8.131 g cm^{-3} [26]. The aim of this work is to develop La–Co–Sn ternary alloys with the high crystal density as anodes for Li-ion batteries. To reach this target, we use Sn to substitute partial Co in the $LaCo_5$ alloy to prepare Sn-rich La–Co–Sn ternary alloys. Finally, electrochemical properties of these La–Co–Sn ternary alloys before and after ball milling as anode materials for Li-ion batteries were performed.

2. Experimental

$LaCo_{5-x}Sn_x$ (x = 3–4.5) alloys were synthesized by arc-melting using excess 10% wt Sn. The as-cast samples were pulverized to 200–400 meshes and alloy powders were further ball-milled. The ball-milling was performed in a planetary ball mill in cyclohexane under Ar atmosphere for different times. A rotation rate was 580 rpm and a charge ratio was 20/1. The microstructure and morphology of the samples were characterized by X-ray diffraction (XRD, Rigaku D/max-2500) and scanning electron microscopy (SEM, Hitachi S3500N).

The working electrodes were prepared by mixing alloy powders, acetylene black and polytetrafluoroethylene (PTFE) at the weigh

* Corresponding author. Tel.: +86 22 23500876; fax: +86 22 23500876.
E-mail address: xpgao@nankai.edu.cn (X.P. Gao).

0378-7753/$ – see front matter © 2008 Elsevier B.V. All rights reserved.
doi:10.1016/j.jpowsour.2008.09.055

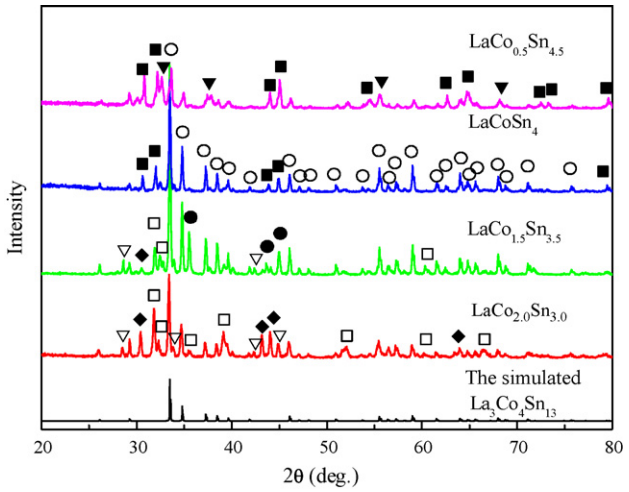

Fig. 1. XRD patterns of the as-cast $LaCo_{5-x}Sn_x$ ternary alloys (x = 3–4.5) and the simulated XRD pattern of pristine $La_3Co_4Sn_{13}$ (○ $La_3Co_4Sn_{13}$; □ $Co_2La_3Sn_7$; ♦ Co_3Sn_2; ▽ CoSn; ● $CoSn_2$; ■ Sn; ▼ $LaSn_3$).

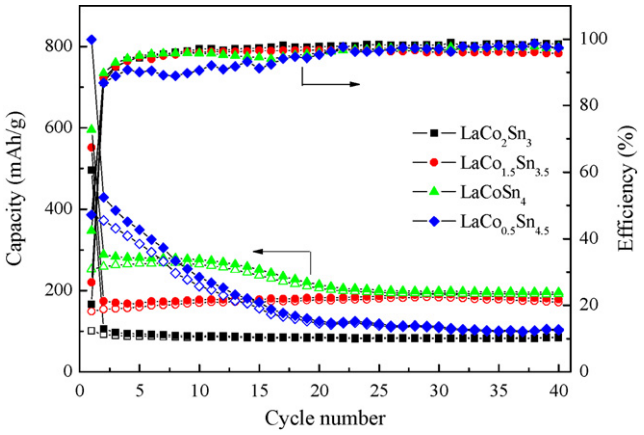

Fig. 2. Cycle performance of the as-cast $LaCo_{5-x}Sn_x$ (x = 3–4.5) ternary alloys at the current density of 50 mA g^{-1} in the potential window of 0.01–2.0 V (vs. Li^+/Li). (solid: discharge capacity; open: charge capacity).

ratio of 70:20:10 into paste, then by roll pressing the paste into a film, and finally by pressing the film onto a Cu foil current collector. The working electrodes were dried at 80 °C for 12 h in vacuum (10^{-3} Torr). A Li metal foil was used as the counter and reference electrode. The electrolyte was 1 M $LiPF_6$ in a mixture of ethylene carbonate (EC), propylene carbonate (PC), and dimethyl carbonate (DMC). The volume ratio of EC:PC:DMC in the mixture was 6:3:1. The cells were assembled in an atmosphere of high-purity argon in a glove box. Discharge/charge measurements of the cells were carried out at the current density of 50 mA g^{-1} between the potential range of 0.01–2.0 V (vs. Li^+/Li) using a LAND-CT2001A instrument. Cyclic voltammograms (CVs) and electrochemical impedance spectra (EIS) were carried out using an IM6ex electrochemical workstation at room temperature.

3. Results and discussion

XRD patterns of the as-cast $LaCo_{5-x}Sn_x$ (x = 3–4.5) are shown in Fig. 1, and the simulated XRD pattern of pristine $La_3Co_4Sn_{13}$ phase is also presented according to previous report [26]. It is clear that all the as-cast $LaCo_{5-x}Sn_x$ (x = 3–4.5) alloys have a multiphase structure. The $La_3Co_4Sn_{13}$ phase with the $Yb_3Rh_4Sn_{13}$ structure-type as the main phase exists in all the as-cast $LaCo_{5-x}Sn_x$ alloys, suggesting that the $La_3Co_4Sn_{13}$ phase is a common phase in Sn-rich La–Co–Sn ternary alloys. Compared to the pattern of the pristine $La_3Co_4Sn_{13}$ phase, some diffraction peaks (2θ = 31.8, 32.3, 35.5, 39.1, 51.6, 60.2 and 66.4°) appear in patterns of $LaCo_2Sn_3$ and $LaCo_{1.5}Sn_{3.5}$ alloys, corresponding to the $Co_2La_3Sn_7$ phase with orthorhombic structure (JCPDS Card No. 51-0645). Meanwhile, the $Co_2La_3Sn_7$ fraction decreases and the $La_3Co_4Sn_{13}$ fraction increases with increasing the Sn amount in alloys. Moreover, a trace of the hexagonal Co_3Sn_2 phase (2θ = 30.4, 43.2, 43.7, 54.5 and 63.4°) and the CoSn phase (2θ = 28.5, 33.8, 40, 42.3 and 44.9°) was also observed in XRD pattern of the $LaCo_2Sn_3$ alloy. In the case of the $LaCo_{1.5}Sn_{3.5}$ alloy, the fractions of Co_3Sn_2 and CoSn phases become weak, on the contrary, the tetragonal $CoSn_2$ phase (2θ = 35.5, 43.6 and 45°) appears instead. When the Sn amount is further increased to 4 and 4.5, the $Co_2La_3Sn_7$ phase almost disappears. In addition, some peaks (2θ = 30.8, 32.2, 44 and 45.1°), corresponding to tetragonal Sn, were found in XRD patterns of $LaCoSn_4$ and $LaCo_{0.5}Sn_{4.5}$ alloys. Simultaneously, the cubic $LaSn_3$ phase (2θ = 32.6, 37.8, 54.5 and 68.1°) also appears.

The cycle performance of as-cast $LaCo_{5-x}Sn_x$ (x = 3–4.5) ternary alloys is presented in Fig. 2. The initial discharge capacities of as-cast $LaCo_2Sn_3$, $LaCo_{1.5}Sn_{3.5}$, $LaCoSn_4$ and $LaCo_{0.5}Sn_{4.5}$ alloys are 495.8, 551.6, 595.0 and 816.8 mAh g^{-1}, respectively. The increase in their initial discharge capacities with increasing the Sn amount in alloys is mainly attributed to the high lithium storage capacity of Sn. In following cycles, except of the $LaCo_{0.5}Sn_{4.5}$ alloy, the as-cast $LaCo_2Sn_3$, $LaCo_{1.5}Sn_{3.5}$ and $LaCoSn_4$ alloys can exhibit the good cycle *performance*. The more rapid capacity fade for the Sn-rich alloy electrode is mainly attributed to the inhomogeneous volume expansion of the bulk alloy during lithium alloying/de-alloying processes with higher lithium content. However, it is noted that the reversible capacity is unsatisfied as compared with that of Sn–Co amorphous alloys published [12,13]. Among these as-cast La–Co–Sn ternary alloys, the $LaCoSn_4$ alloy seems to exhibit a higher reversible capacity and a better cycle ability. Therefore, the $LaCoSn_4$ alloy is selected to further improve the electrochemical performance after ball-milling process, based on decreasing the crystallinity of the alloy.

XRD patterns of the as-cast $LaCoSn_4$ alloy and ball-milled $LaCoSn_4$ alloys for different times are shown in Fig. 3. Evidently, the diffraction peaks of the $La_3Co_4Sn_{13}$ phase are broadened and merged after ball-milling for 8–16 h, indicating the *reduced* crys-

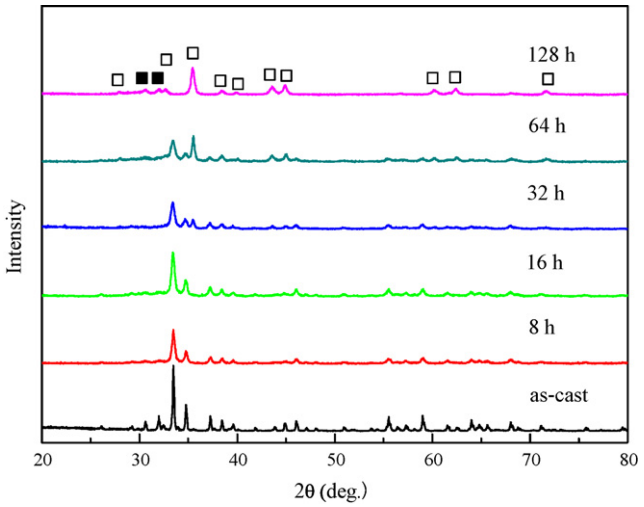

Fig. 3. XRD patterns of the as-cast $LaCoSn_4$ alloy and ball-milled $LaCoSn_4$ alloys for different times (□ $CoSn_2$; ■ Sn).

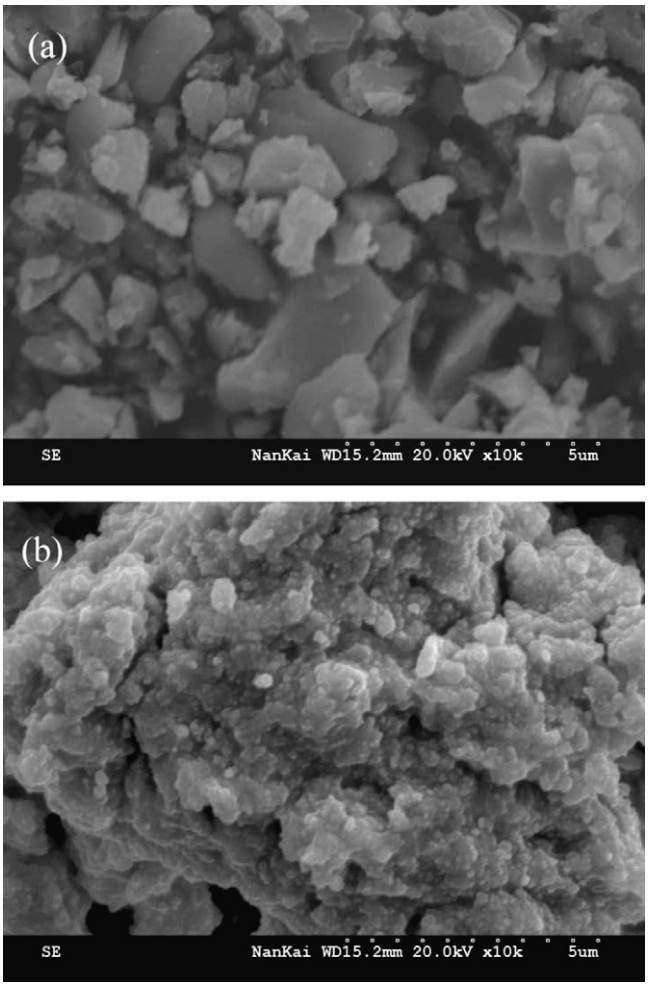

Fig. 4. SEM images of the as-cast $LaCoSn_4$ alloy (a) and ball-milled $LaCoSn_4$ alloys for 16 h (b).

tallinity of the alloy induced during ball-milling. After further ball-milling to 32 h, a new $CoSn_2$ phase is gradually formed and become the main phase after ball-milling for 64 h. While ball-milling is conducted for 128 h, the obtained product can be only indexed to $CoSn_2$ with a trace of Sn. The reason is probably due to the gradual decomposition of the $La_3Co_4Sn_{13}$ phase into the Co–Sn phase and the La–Sn phase after ball-milling for a long time. Moreover, the amorphous transformation is happened to a certain extent for the solid solution La–Sn phase during ball-milling, as compared to Co–Sn phase.

SEM images of the as-cast $LaCoSn_4$ alloy and ball-milled $LaCoSn_4$ alloys for 16 h are illustrated in Fig. 4. The surface morphology of the $LaCoSn_4$ alloy before and after ball-milling treatment is obviously different. The as-cast $LaCoSn_4$ alloy powders have an average particle size of 3–5 μm with clear edges and corners. However, after ball-milling, the sample *has* an irregular agglomerated morphology with small particles, showing the *reduced* crystallinity as demonstrated in XRD analysis.

Fig. 5 shows the initial charge/discharge profiles of the $LaCoSn_4$ alloys after ball-milling for different times. As expected, the initial discharge capacities are significantly enhanced for ball-milled alloys. The initial discharge capacities are 976.6, 891.8, 842.8, 880.7 and 843 mAh g^{-1} for the $LaCoSn_4$ alloys after ball-milling for 8, 16, 32, 64 and 128 h, respectively, which are much higher than that of the as-cast $LaCoSn_4$ alloy. It means that ball-milling process can produce more new active sites for lithium alloying. The declining

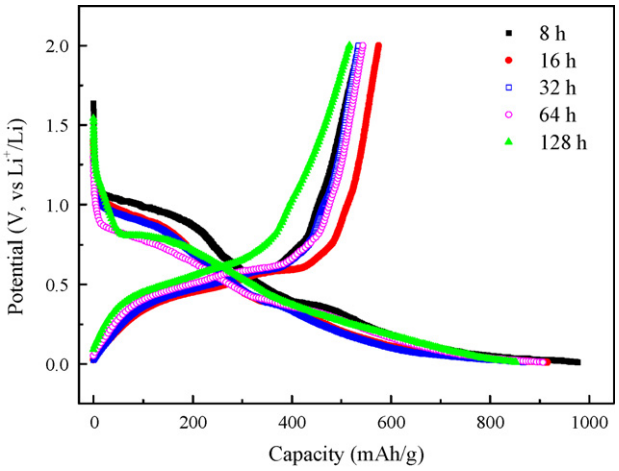

Fig. 5. Initial charge/discharge profiles of the $LaCoSn_4$ alloy after ball-milling for different times at the current density of 50 mA g^{-1}.

plateau at the high potential of 1.0–0.5 V, which consume quite a few of the discharge capacity (~300 mAh g^{-1}), should contain the formation of SEI film and initial structural rearrangement of ball-milled alloys. These multi-step processes can overlap in the potential profile [27].

The cycle performance of the $LaCoSn_4$ alloy after ball-milling for different times is depicted in Fig. 6. All the ball-milled alloys have the enhanced discharge capacity and the improved cycle *performance* as compared to the as-cast alloy. The capacity increases during the first 10 cycles, then remains the good stability between the 10th and 30th cycle, and finally decreases slowly after the 30th cycle. The similar behavior was also observed in other tin-based alloy anodes [28–30]. The activation process during the first 10 cycles is attributable to the incomplete structure–destruction process during cycling. The discharge capacities are 489, 534.9, 545.9 and 507.9 mAh g^{-1} after 40 cycles for $LaCoSn_4$ alloys after ball-milling for 8, 16, 32 and 64 h, respectively. However, the capacity of the alloy, obtained after ball-milling for 128 h, decreases rapidly to 394.4 mAh g^{-1} after 40 cycles. This is probably due to the gradual decomposition of the $La_3Co_4Sn_{13}$ phase into the Co–Sn phase and the La–Sn phase after ball-milling for long time *as shown in XRD patterns*. By comparison, the ball-milled $LaCoSn_4$ alloy for 16 h is shown to have the *best* electrochemical performance. However, it should be noted that the large irreversible capacity losses of these

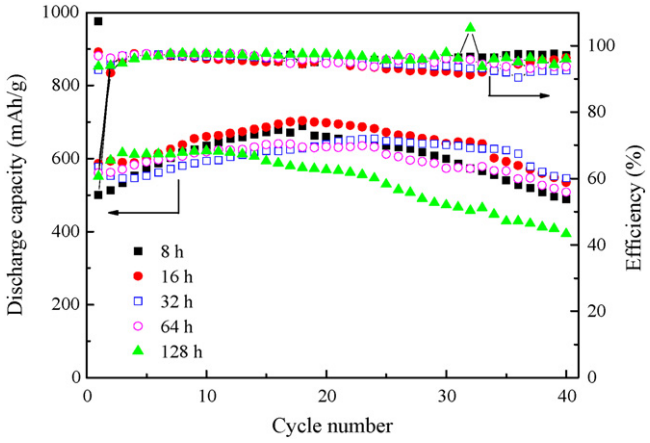

Fig. 6. Cycle performance of the $LaCoSn_4$ alloy after ball-milling for different times at the current density of 50 mA g^{-1}.

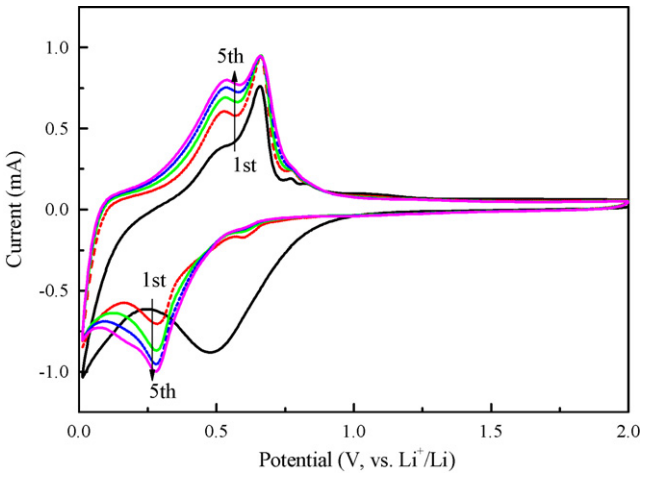

Fig. 7. Cyclic voltammograms of the $LaCoSn_4$ alloy after ball-milling for 16 h in the potential range from 0.01 to 2.0 V (vs. Li^+/Li) at the scan rate of 0.1 mV s^{-1}.

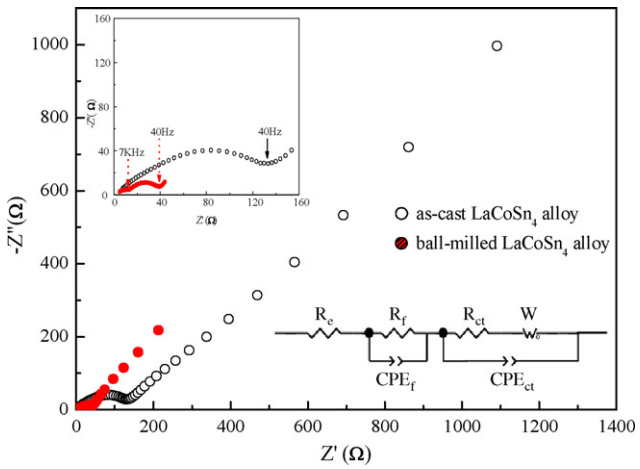

Fig. 8. Electrochemical impedance spectra of the as-cast alloy and ball-milled $LaCoSn_4$ alloy for 16 h after the 5 cycles. Inset shows the equivalent circuit.

materials in the first cycle are still observed, which have a negative impact on their potential application. Except for the formation of SEI film, the low efficiency of acetylene black (about 25%) as additive is related to the large irreversible capacity losses, which can be also observed in metal oxide-acetylene black [31]. Further increase the coulombic efficiency in the first cycle is necessary for these materials.

Fig. 7 shows the cyclic voltammograms (CV) of the $LaCoSn_4$ alloy after ball-milling for 16 h. In the first cathodic process, there are two reduction peaks at 0.45 and 0.01 V (vs. Li^+/Li), respectively. One cathodic peak at 0.45 V (vs. Li^+/Li) with the onset potential at about 1.0 V in the first cycle, which is related to the discharge potential plateau in Fig. 5, disappears in the following cycles. The ball-milling may induce lattice defects and *reduced* crystallinity of the $LaCoSn_4$ alloy, which can capture more charges for the SEI formation, leading to the appearance of the large irreversible cathodic peak. The SEI film formed will be stable under subsequent lithium alloying and de-alloying processes [32]. After following cycles, the cathodic peak is stabilized at 0.28 V (vs. Li^+/Li), indicating the stable lithium alloying process. Subsequent anodic process up to 2.0 V show three oxidation peaks at 0.52, 0.65 and 0.78 V, corresponding to the gradual de-alloying process in the first cycle. The gradual increase of the peak current in CV-loops further confirms the existence of the activation process in Fig. 6.

To further understand the improved electrochemical performance of the ball-milled $LaCoSn_4$ alloy for 16 h, electrochemical impedance spectra (EIS) of the as-cast and the ball-milled $LaCoSn_4$ alloys are performed and illustrated in Fig. 8. Both Nyquist plots consist of two semicircles at high/medium frequency regions, and a straight line at a low frequency region. The semicircle in the medium frequency region is attributed to the charge-transfer reaction of the alloy, and the inclined line corresponds to the lithium-ion diffusion process (Warburg impedance) within electrode [33,34]. Both the charge-transfer resistance (R_{ct}) and the Warburg impedance (W) of the ball-milled alloy are much lower than that of the as-cast alloy, which are beneficial to the great improvement of the electrochemical performance. Usually, the charge-transfer resistance is attributed to the surface active sites of the electrode materials, while the Warburg impedance is mainly related to the diffusion path within the electrode materials. This indicates that the ball-milling process results in the *reduced* crystallinity, grain size, short diffusion path of the electrode materials, and the subsequent decrease of both the charge-transfer resistance and the Warburg impedance for lithium alloying/de-alloying processes. Correspondingly, the discharge capacities of the ball-milled alloys increase obviously.

4. Conclusion

In summary, Sn-rich La–Co–Sn ternary alloys were obtained by arc-melting process and subsequent ball-milling. All the as-cast La–Co–Sn ternary alloys have the same main phase of $La_3Co_4Sn_{13}$ and low electrochemical capacities. Among these alloys, the as-cast $LaCoSn_4$ alloy seems to exhibit optimized electrochemical performance. The ball-milling process results in the *reduced* cystallinity and the partial decomposition of the alloys. All ball-milled alloys can deliver enhanced electrochemical capacities as compared to the as-cast alloy, which is further confirmed by EIS analysis. In particular, the $LaCoSn_4$ alloy ball-milled for 16 h provides the higher discharge capacity of 500 mAh g^{-1} after 40 cycles. Although further studies are required to understand and increase the coulombic efficiency in the initial cycle, La–Co–Sn ternary alloys with the high crystal density can be considered as promising anode materials for lithium-ion batteries.

Acknowledgment

This work is supported by the 973 Program (2009CB220100), China.

References

[1] J.M. Tarascon, M. Armand, Nature 414 (2001) 359.
[2] J.R. Dhan, T. Zheng, Y. Liu, J.S. Xue, Science 270 (1995) 590.
[3] M. Winter, J.O. Besenhard, M.E. Spahr, P. Novak, Adv. Mater. 10 (1998) 725.
[4] Y. Idota, T. Kubota, A. Matsufuji, Y. Maekawa, T. Miyasaka, Science 276 (1997) 1395.
[5] J. Yang, M. Winter, J.O. Besenhard, Solid State Ionics 90 (1996) 281.
[6] I.A. Courtney, J.R. Dahn, J. Electrochim. Soc. 144 (1997) 2045.
[7] I.S. Kim, J.T. Vaughey, O. Auciello, J. Electrochem. Soc. 155 (2008) A448.
[8] L. Fang, B.V.R. Chowdari, J. Power Sources 97–98 (2001) 181.
[9] H. Sakauchi, H. Maeta, M. Kubota, H. Honda, T. Esaka, Electrochemistry 68 (2000) 632.
[10] O. Mao, R.A. Dunlap, J.R. Dahn, J. Electrochem. Soc. 146 (1999) 405.
[11] H. Mukaibo, T. Sumi, T. Yokoshima, T. Momma, T. Osaka, Electrochem. Solid State Lett. 6 (2003) A218.
[12] N. Tamura, M. Fujimoto, M. Kamino, S. Fujitani, Electrochim. Acta 49 (2004) 1949.
[13] J.J. Zhang, Y.Y. Xia, J. Electrochem. Soc. 153 (2006) A1466.
[14] D. Larcher, L.Y. Beaulieu, D.D. Macneil, J.R. Dahn, J. Electrochem. Soc. 147 (2000) 1658.
[15] F.S. Ke, L. Huang, J.S. Cai, S.G. Sun, Electrochim. Acta 52 (2007) 6741.
[16] H. Li, L.H. Shi, W. Lu, X.J. Huang, L.Q. Chen, J. Electrochem. Soc. 148 (2001) A915.

[17] H. Sakaguchi, H. Honda, Y. Akasaka, T. Esaka, J. Power Sources 119–121 (2003) 50.
[18] O. Mao, J.R. Dahn, J. Electrochem. Soc. 146 (1999) 414.
[19] S. Matsuno, T. Kohno, N. Takami, F. Kawashima, T. Sawa, Electrochem. Solid-State Lett. 8 (2005) A234.
[20] S.D. Beattie, J.R. Dahn, J. Electrochem. Soc. 152 (2005) C542.
[21] E. Ronnebro, J.T. Yin, A. Kitano, M. Wada, S. Tanase, T. Sakai, J. Electrochem. Soc. 152 (2005) A152.
[22] J.J. Zhang, X. Zhang, Y.Y. Xia, J. Electrochem. Soc. 154 (2007) A7.
[23] J.T. Vaughey, J. Owejan, M.M. Thackeray, Electrochem. Solid State Lett. 10 (2007) A220.
[24] H. Guo, H.L. Zhao, X. Ha, H.C. He, W.H. Qiu, X. Li, J. Power Sources 174 (2007) 921.
[25] X.N. Zhang, P.X. Huang, G.R. Li, T.Y. Yan, G.L. Pan, X.P. Gao, Electrochem. Commun. 9 (2007) 713.
[26] E.L. Thomas, H.O. Lee, A.N. Bankston, S. MaQuilon, P. Klavins, M. Moldovan, D.P. Young, Z. Fisk, F.J. Chan, J. Solid State Chem. 179 (2006) 1642.
[27] L.F. Nazar, G. Goward, F. Leroux, M. Duncan, H. Hung, T. Kerr, J. Gaubicher, Int. J. Inorg. Chem. 3 (2001) 191.
[28] L.J. Ning, N.P. Wu, S.B. Fang, E. Rahm, R. Holze, J. Power Sources 133 (2004) 229.
[29] H. Guo, H.L. Zhao, X.D. Jia, Electrochem. Commun. 9 (2007) 2207.
[30] H.C. Shin, M. Liu, Adv. Funct. Mater. 15 (2005) 582.
[31] B.T. Hang, T. Doi, S. Okada, J.I. Yamaki, J. Power Sources 174 (2007) 493.
[32] G.X. Wang, J.H. Ahn, J. Yao, S. Bewlay, H.K. Liu, Electrochem. Commun. 6 (2004) 689.
[33] N. Sharma, J. Plevert, G.V. Subba, B.V.R. Chowdari, T.J. White, Chem. Mater. 17 (2005) 4700.
[34] M.S. Park, Y.M. Kang, G.X. Wang, S.X. Dou, H.K. Liu, Adv. Funct. Mater. 18 (2008) 455.